The Astrophysical Journal Letters, 774:L29 (6pp), 2013 September 10 doi:10.1088/2041-8205/774/2/L29

DETECTION OF EQUATORWARD MERIDIONAL FLOW AND EVIDENCE OF DOUBLE-CELL MERIDIONAL CIRCULATION INSIDE THE SUN

Junwei Zhao[1], R. S. Bogart[1], A. G. Kosovichev[1], T. L. Duvall, Jr.[2], and Thomas Hartlep[1]
[1] W. W. Hansen Experimental Physics Laboratory, Stanford University, Stanford, CA 94305-4085, USA
[2] Solar Physics Laboratory, NASA Goddard Space Flight Center, Greenbelt, MD 20771, USA
Received 2013 June 21; accepted 2013 July 30; published 2013 August 27

ABSTRACT

Meridional flow in the solar interior plays an important role in redistributing angular momentum and transporting magnetic flux inside the Sun. Although it has long been recognized that the meridional flow is predominantly poleward at the Sun's surface and in its shallow interior, the location of the equatorward return flow and the meridional flow profile in the deeper interior remain unclear. Using the first 2 yr of continuous helioseismology observations from the *Solar Dynamics Observatory*/Helioseismic Magnetic Imager, we analyze travel times of acoustic waves that propagate through different depths of the solar interior carrying information about the solar interior dynamics. After removing a systematic center-to-limb effect in the helioseismic measurements and performing inversions for flow speed, we find that the poleward meridional flow of a speed of 15 m s^{-1} extends in depth from the photosphere to about 0.91 $R_\odot$. An equatorward flow of a speed of 10 m s^{-1} is found between 0.82 and 0.91 $R_\odot$ in the middle of the convection zone. Our analysis also shows evidence of that the meridional flow turns poleward again below 0.82 $R_\odot$, indicating an existence of a second meridional circulation cell below the shallower one. This double-cell meridional circulation profile with an equatorward flow shallower than previously thought suggests a rethinking of how magnetic field is generated and redistributed inside the Sun.

Key words: Sun: helioseismology – Sun: interior – Sun: oscillations

Online-only material: color figures

1. INTRODUCTION

Meridional flow inside the Sun plays an important role in redistributing rotational angular momentum and transporting magnetic flux (Wang et al. 1989), and is crucial to our understanding of the strength and duration of sunspot cycles (Hathaway & Rightmire 2010; Dikpati et al. 2010) according to flux-transport dynamo theories (Choudhuri et al. 1995; Dikpati & Charbonneau 1999). At the Sun's surface and in its shallow interior to at least 30 Mm in depth, the meridional flow is predominantly poleward with a peak speed of approximately 20 m s^{-1}, as measured by tracer tracking (e.g., Komm et al. 1993; Švanda et al. 2007; Hathaway & Rightmire 2010), direct Doppler-shift observations (e.g., Ulrich 2010), and local helioseismology analyses (e.g., Giles et al. 1997; Haber et al. 2002; Zhao & Kosovichev 2004; González Hernández et al. 2008). The poleward plasma flow transports the surface magnetic flux from low latitudes to the polar region, causing the periodic reversals of the global magnetic field, a process important to the prediction of the solar cycles (Dikpati et al. 2010). The speed and variability of the meridional flow also play an important role in determining the strength and duration of the solar cycles, and the unusually long activity minimum at the end of Solar Cycle 23 during 2007–2010 was thought to be associated with an increase of the meridional flow speed during the declining phase of the previous cycle (Hathaway & Rightmire 2010). Therefore, an accurate determination of the meridional flow profile is crucial to our understanding and prediction of solar magnetic activities.

Although the poleward meridional flow at the solar surface and in shallow depths has been well studied, the depth and speed profile of the equatorward return flow, which is expected to exist inside the solar convection zone to meet the mass conservation, largely remains a puzzle. It is generally assumed that the return flow is located near the base of the convection zone, although no convincing evidence has been reported. Earlier helioseismic analyses of *Solar Heliospheric Observatory*/Michelson Doppler Imager (*SOHO*/MDI; Scherrer et al. 1995) data were unable to directly detect an equatorward flow, but estimated that the return flow had a speed of 2 m s^{-1} near the bottom of the convection zone after applying a mass-conservation constraint (Giles 1999). This single-cell circulation profile has been later widely employed in the flux-transport dynamo simulations and solar cycle prediction models (e.g., Dikpati et al. 2010; Jiang et al. 2007). A later helioseismic frequency-shift analysis put the equatorward flow at a much shallower depth of 40 Mm (Mitra-Kraev & Thompson 2007), but this was questioned by Gough & Hindman (2010). More recently, an analysis based on tracking of photospheric supergranulation gave an estimate of the return flow depth below 50 Mm (Hathaway 2012), however, this analysis was unable to give an unambiguous profile of the meridional circulation as a function of both latitude and depth inside the Sun. A more robust analysis utilizing a well-established helioseismology technique, e.g., time–distance helioseismology (Duvall et al. 1993), is needed to examine the deep meridional circulation profile.

The continuous Doppler observations by the Helioseismic and Magnetic Imager (HMI; Scherrer et al. 2012; Schou et al. 2012) onboard the recently launched *Solar Dynamics Observatory* mission (*SDO*; Pesnell et al. 2012) allow us to measure and detect the long-sought equatorward flow. Our analysis, which takes into account the systematic center-to-limb effect that was recently found in the local helioseismology analysis techniques (Zhao et al. 2012), gives a two-dimensional cross-section picture of the meridional flow inside the nearly entire solar convection zone, and reveals a double-cell circulation with the equatorward flow located near the middle of the convection zone. In this Letter, we describe our analysis procedure in Section 2, present

measurements and inversion results in Section 3, and then discuss these results in Section 4.

2. DATA ANALYSIS

The *SDO*/HMI provides continuous full-disk Doppler-shift observations of the Sun with a 45 s cadence for helioseismology studies. Time–distance helioseismology (Duvall et al. 1993) measures travel times of acoustic waves, which propagate through the solar interior, by cross-correlating oscillation signals observed at different locations on the surface. The measured travel-time anomalies are usually interpreted in terms of wave-speed perturbations and mass flows along the wave path. This analysis technique has already provided rich information about the solar interior structures and dynamics (Gizon et al. 2010).

Determining the internal meridional flow is one important task in solar physics and yet one difficult challenge due to the low speed of the flow, which requires a careful analysis of potential systematic errors. In particular, recent studies have revealed a previously unreported systematic center-to-limb effect in the acoustic travel times measured by the time–distance technique (Zhao et al. 2012). The systematic travel-time variation depends on the angular distance from the solar disk center, and exhibits different magnitude, sometimes even opposite signs, when measured using different HMI observables and using different measurement distances. It is not quite clear what causes this systematic effect, and a recent study suggested that it might be partially due to the interactions of acoustic waves with the vertical flows in solar granules (Baldner & Schou 2012). Zhao et al. (2012) suggested that this systematic effect should be removed before inverting the measured acoustic travel times for interior meridional flow, and proposed to use the travel-time shifts measured in the east–west direction along the equator as proxies of the systematic effect. Their inversion results, after removal of this effect following their suggested method, showed a reduction of $\sim$10 m s^{-1} in the inverted meridional flow speed (Zhao et al. 2012). We believe that this systematic effect was responsible for many past helioseismology study failures to reliably detect the equatorward meridional flow, and that the removal of this effect will play an important role in studying the meridional flow in the solar interior.

We use the HMI Doppler-shift data covering its first 2 yr period from 2010 May 1 through 2012 April 30, during which the solar magnetic activity was generally low. For each observing day, we track the data with a uniform Carrington rotation rate, remap the tracked data onto the heliographic coordinate using Postel's projection with a sampling scale of $0\overset{\circ}{.}18$ pixel^{-1}, and then apply a running-difference filter to remove solar convection and low-frequency signals. Note that no other filtering is applied in our analysis in order to avoid any complications in the Fourier domain when dealing with very large spatial scales. A deep-focusing time–distance measurement scheme (shown in Figure 1), which was described and validated by Hartlep et al. (2013), is utilized. For each measurement, the solar oscillation signals are first averaged inside two 30°-long single-pixel-wide concentric arcs, located opposite to each other in the north and south directions, and then cross-correlated to extract acoustic wave packets traveling between these arcs along the wave paths through the solar interior. In order to make a robust center-to-limb effect correction, we limit the selection of oscillation signals within 15° from the central meridian. The center-to-limb variations are estimated from the east–west travel-time measurements along an equatorial band following the same geometry as used in the north–south measurements along the meridian band. The same procedure is repeated for each of the 60 measurement distances ranging from $2\overset{\circ}{.}16$ to $44\overset{\circ}{.}64$, covering a radial range from approximately 0.7 $R_\odot$ to the surface according to the acoustic ray theory. The cross-correlation functions are averaged for the same latitudes, and then averaged again over one month intervals. The Gabor wavelet fitting (Kosovichev & Duvall 1997) is performed to derive the acoustic travel times for all the measurement distances. For each distance, the travel times are averaged again over the whole 2 yr period to obtain the final results. The standard errors after the systematic effect correction for each measurement distance, estimated from the 24 measurement periods, are displayed as error bars in Figures 2 and 3. The errors of the center-to-limb effect follow a similar pattern as in $\delta\tau_{\rm SN}$.

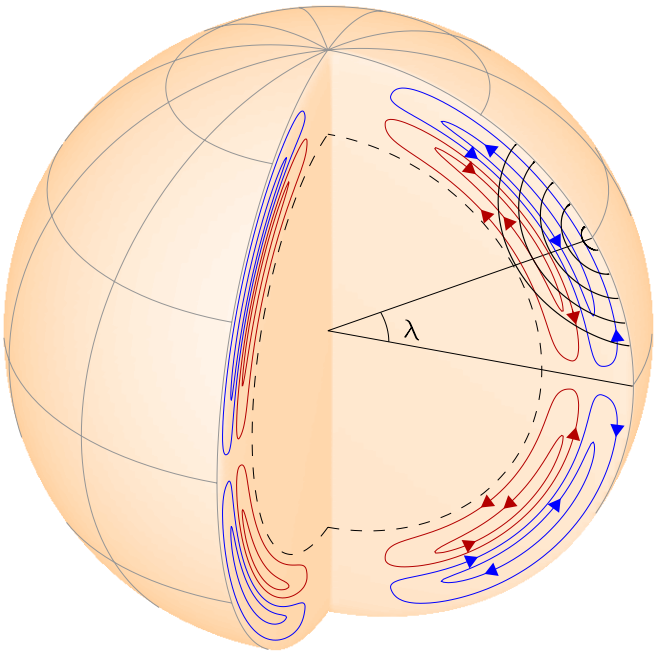

Figure 1. Diagram of the deep-focusing time–distance measurement scheme, with black curves showing some samples of acoustic wave paths. Blue and red streamlines show a schematic structure of the meridional circulation illustrating our results. Black dashed lines show the bottom of the convection zone at 0.7 $R_\odot$. (A color version of this figure is available in the online journal.)

3. RESULTS

3.1. Results of Travel-time Measurements

Figure 2 shows some selected examples of $\delta\tau_{\rm SN}$, which is defined as the travel-time differences between the southward and northward propagating acoustic waves after corrected for the systematic center-to-limb variation, as a function of latitude. A small systematic offset caused by the imperfect alignment of the HMI instrument relative to the solar rotation axis is also removed following the same approach by Giles et al. (1997) and Hathaway & Rightmire (2010). Examples of $\delta\tau_{\rm SN}$ as functions of the measurement distance, or radius of the lower turning point of acoustic wave paths estimated from acoustic ray-path approximation, for selected latitudes are shown in Figure 3(a). The $\delta\tau_{\rm SN}$, caused by the internal meridional flows, are of an order of 1 s for short distances (corresponding to the wave paths confined to the shallow interior and reflecting the shallow poleward flow), and decrease rapidly with the measurement

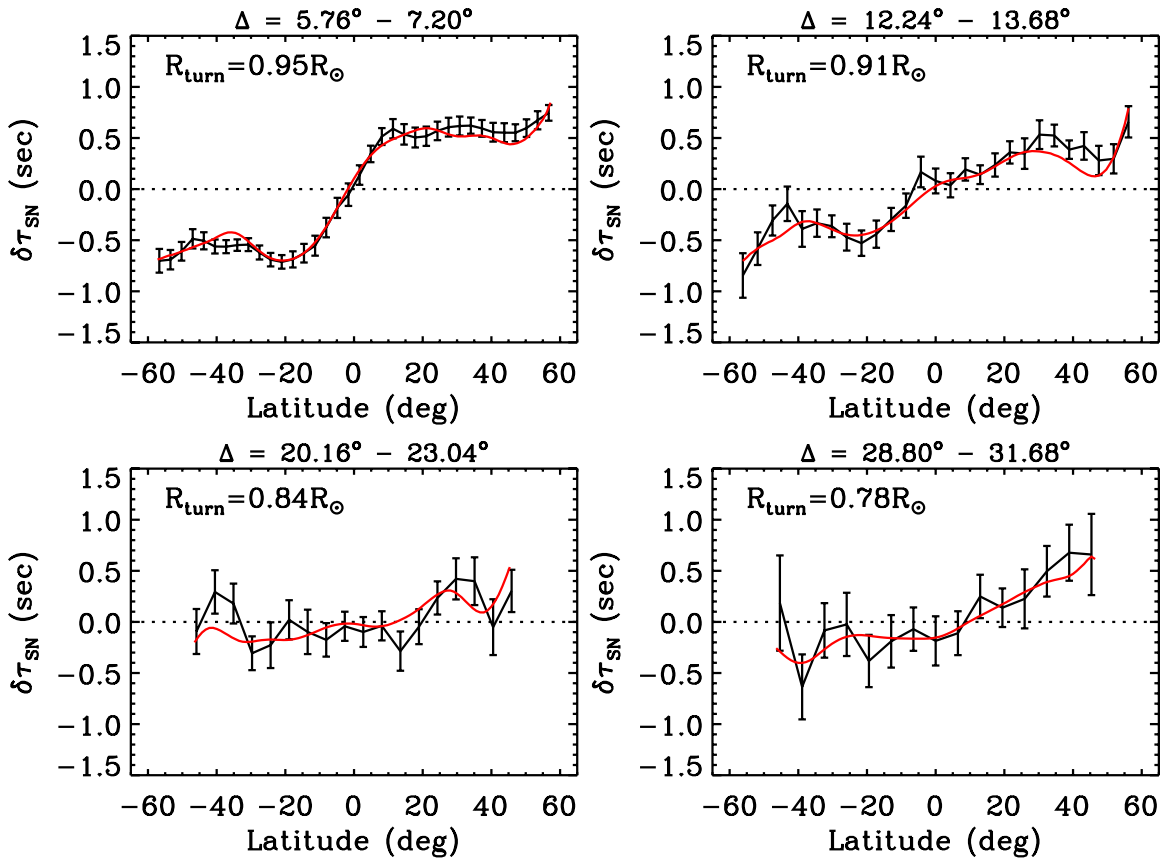

Figure 2. Measured acoustic travel-time differences, $\delta\tau_{\rm SN}$, shown as black curves for selected measurement distances. The measurement distances Δ and corresponding radii of acoustic wave lower turning points, $R_{\rm turn}$, which are derived from the ray-path approximation, are marked in each panel. Red curves are the $\delta\tau_{\rm SN}$ calculated from our inversion results displayed in Figure 4, showing that our inversion results fit the measurements well. Error bars for the red curves are similar to those for the black curves.

(A color version of this figure is available in the online journal.)

distance (or the turning-point radius). The values of $\delta\tau_{\rm SN}$ drop close to zero and even change sign for certain latitudes, and then become to increase again. This trend is essentially the same for both hemispheres, although there are clear differences between the two.

To gain more confidence in these measurements and the procedure correcting the systematic effect, we also analyze the Doppler-shift data acquired by *SOHO*/MDI (Scherrer et al. 1995). MDI observed the Sun from 1996 through 2011, and its Dynamics Program, usually lasting two months each year, had continuous full-disk Doppler-shift observations for helioseismic studies. To avoid complications caused by solar magnetic activity and for the purpose of a better comparison with the HMI results obtained during a relatively quiet period, we select the MDI Dynamics Program data from the solar minimum years of 1996–1998 and 2006–2010, and perform the analysis following the exactly same procedure as we do for HMI data. Note that although the full-disk data from HMI and MDI have different spatial resolutions, both data are remapped to a lower resolution of $0.^{\circ}18$ pixel^{-1} before being used for the helioseismic analysis. We find that despite the differences in the observed spectral lines and different observing periods, the $\delta\tau_{\rm SN}$ from the two instruments are in reasonable agreement after the systematic effect correction (Figure 3(a)). It is worth pointing out that the original measurements of $\delta\tau_{\rm SN}$ from both instruments differ substantially before the removal of the center-to-limb effect (Figure 3(b)). This indicates that the center-to-limb variations from the HMI and MDI are significantly different, which is believed to be because they observe different spectral lines, and also shows that our procedure to remove the systematic effect is reasonable and robust.

3.2. Results from Inversion

We then invert the corrected $\delta\tau_{\rm SN}$ from HMI for the interior meridional flow speed as a function of latitude and depth. Ray-approximation sensitivity kernels are utilized in the inversion, and they are prepared following the same geometry and averaging procedures as in the measuring. Three-dimensional kernels are first computed in spherical coordinates, and then collapsed into one meridional plane. Basically, the sensitivity kernels show thin curves of the ray path, with the strongest sensitivity located near the lower turning points. We linearize the equation that links the travel-time variations with the interior flow field: $\delta\tau_{\rm diff} = -2\int_{\Gamma}(\mathbf{n}\cdot\mathbf{v})/c^2 d\,s$, where Γ is acoustic ray path, $\mathbf{v}$ is flow velocity, c is sound speed, and s is distance along the ray path (Kosovichev 1996). The linearized equations are then solved in a sense of least squares using the LSQR algorithm, an iterative linear equation solver (Paige & Saunders 1982). In our inversions, the radial component of the flow is not taken into account but it is not expected that this will affect our inversion results significantly because the flows are predominantly horizontal near the deep-focus points where our measurement is more sensitive. However, an inversion procedure including the radial flow will be developed in our future studies.

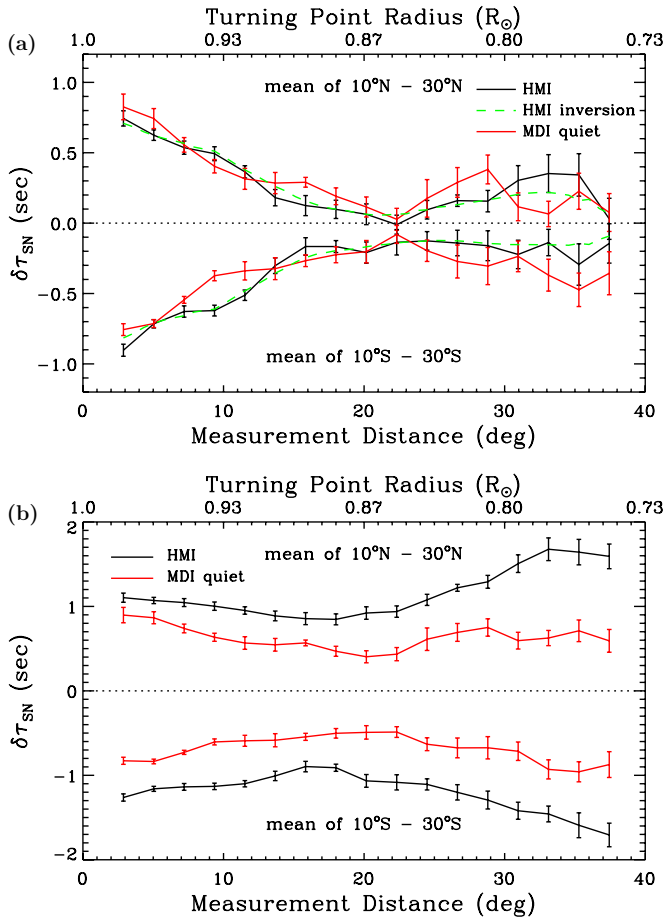

Figure 3. (a) Comparison of the measured acoustic travel-time differences, $\delta\tau_{SN}$, from the HMI and MDI data after removal of the systematic center-to-limb variations, together with the $\delta\tau_{SN}$ calculated from the interior velocity inverted from the HMI measurements. Error bars for the green dashed curves are similar to those for the black curves. (b) Comparison of the $\delta\tau_{SN}$ from the HMI and MDI quiet-period observations before the removal of the systematic effect.

(A color version of this figure is available in the online journal.)

We carry out two sets of inversions with and without the mass-conservation constraint. For the results inverted from only the helioseismic measurements without applying the mass-conservation constraint, a two-dimensional cross-section view of the meridional flow velocity and flow profiles at some selected depths and latitudes are displayed in Figure 4. The $\delta\tau_{SN}$ calculated from a forward procedure, which utilizes the same equation as given above that links travel time and interior flows, using the inverted velocity are overplotted in Figures 2 and 3(a) to compare with the measured $\delta\tau_{SN}$. It can be found that they are in good agreement, demonstrating that our inversion results fit the measurement quite well. Basically, our inversion results show that the poleward flow of 15 m s^{-1} extends from the surface to a depth of approximately 65 Mm, i.e., about 0.91 $R_\odot$. Below this, the flow direction turns equatorward with a maximum speed of about 10 m s^{-1}. Both the depth and the thickness of the zone of return flow are clearly latitude dependent. The equatorward flow shows a significant hemispheric asymmetry, stronger in the northern hemisphere and weaker in the southern. Below about 0.82 $R_\odot$, the flow again becomes poleward, also with a substantial hemispheric asymmetry. Errors from the inversion are typically 1 m s^{-1} near the surface, and are as large as 10 m s^{-1} below 0.80 $R_\odot$. Our inversion stops at about 0.75 $R_\odot$ because the noise prevents reliable inferences in the deeper layers. Longer observations are required to increase the signal-to-noise ratio (S/N).

Another set of inversion with the mass-conservation constraint (results are not shown in a figure) demonstrates that the basic flow profile remains similar to that without applying the mass constraint. The major difference is that the zone of equatorward flow becomes thicker, and the poleward flow below 0.82 $R_\odot$ becomes slower.

The averaging kernels from our inversions for some selected target depths are displayed in Figure 5. It can be seen that the kernel is well localized in the shallow areas, and becomes broader with the increase of depth, but are still localized in the latitudinal direction. The negative side lobes above and below the targeted area in the radial direction also become stronger in amplitude and larger in size with the depth. The averaging kernels remain the same for the same depth but different latitudes.

4. DISCUSSION

Our analysis reveals a new picture of the Sun's interior meridional circulation, with poleward flows from the surface to 0.91 $R_\odot$ and from 0.82 $R_\odot$ to at least 0.75 $R_\odot$, and an equatorward flow located between these in a layer of about 0.09 $R_\odot$ thick. This seems to form two meridional circulation cells, one beneath the other in the radial direction (Figure 1). Not being able to invert the flow profile beneath 0.75 $R_\odot$ and above the latitude of 60°, we cannot exclude the possibility of more circulation cells in both radial and latitudinal directions.

The interior meridional flow profile reported in this Letter is obtained after the removal of the systematic center-to-limb effect, therefore, a precise determination of this flow profile relies largely on a precise determination of that systematic effect. We follow the empirical approach of using the east–west travel-time measurements along the equator to represent this systematic effect, however, without knowing the exact cause of this effect (as already pointed out in Section 2), a small deviation of the real systematic effect from this representation can result in a significant change of the inverted meridional flow profile shown in Figure 4. However, the comparison of MDI and HMI results, which carry different amount of systematic effects, gives us confidence that our effect correction procedure is reasonable (see Figure 3). Still, we believe it is necessary to develop a different systematic-effect correction procedure in the future, after the cause of the center-to-limb effect is better known, to give a more robust inference of the deep meridional flow profile.

Based on a single-cell circulation model with the equatorward flow, peaking at 3 m s^{-1}, located near the bottom of the convection zone, Braun & Birch (2008) estimated that more than one decade of continuous observations is required for a reliable detection of the return flow, which is expected to cause an acoustic travel-time shift of about 0.01 s. However, the meridional flow profile determined from our measurements differs from the model used in their estimation. Furthermore, Figure 3 shows that the travel-time shift caused by the shallow poleward flow is partly offset by the equatorward flow in the middle of the convection zone, leaving the flow near the bottom easier to measure. This explains why 2 yr of helioseismic observations is able to probe the deep interior meridional flow. Certainly, longer observations will enable us to reliably invert

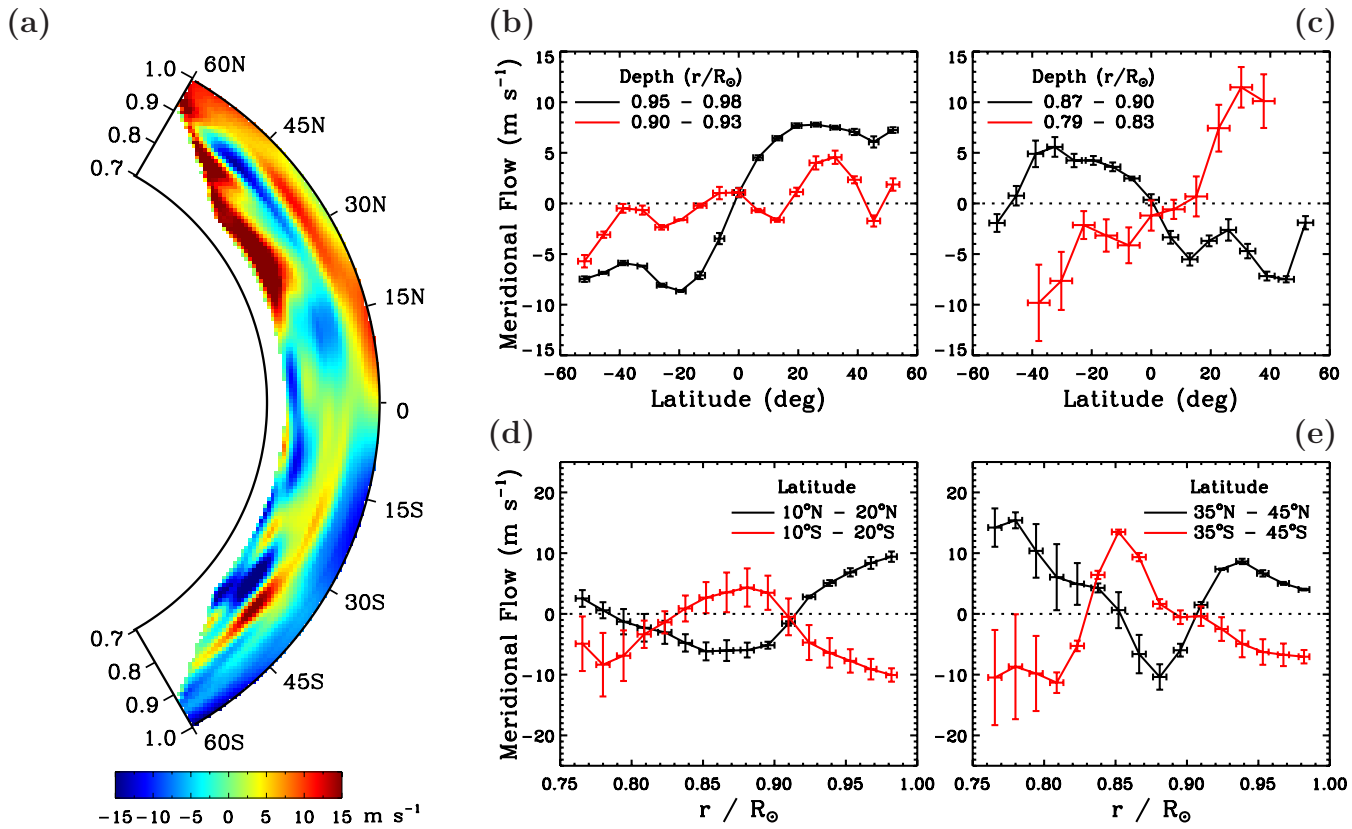

Figure 4. Meridional flow profile, obtained by inverting the measured acoustic travel times. Panel (a) shows a cross-section view of the meridional-flow profile, with the positive velocity directing northward. Panels (b) and (c) show the inverted velocity as functions of latitude averaged over several depth intervals. Panels (d) and (e) show the velocity as functions of depth averaged over different latitudinal bands. Horizontal error bars represent the widths of averaging kernels (as shown in Figure 5) in the latitudinal direction (panels (b) and (c)) and the radial direction (panels (d) and (e)). As the averaging kernels are obtained using the ray-approximation sensitivity kernels without including the finite wavelength effects, these horizontal error bars do not represent the physical sensitivity ranges.

(A color version of this figure is available in the online journal.)

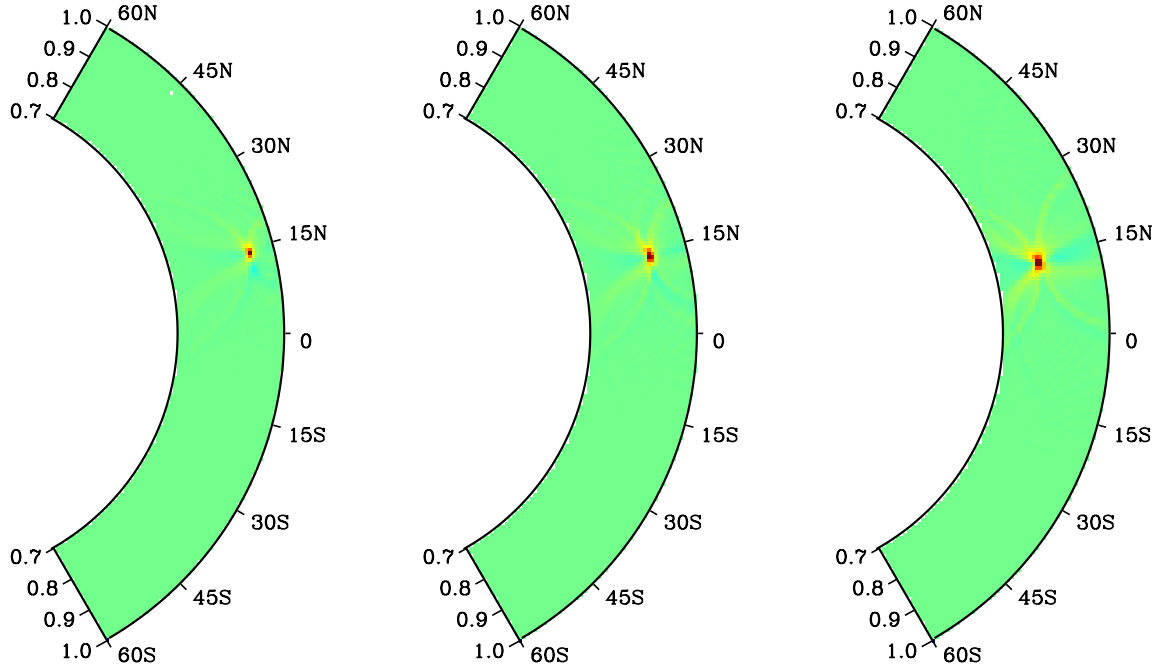

Figure 5. Averaging kernels obtained from the inversion procedure when the target is located at the latitude of 15°N and depths of 50, 75, and 125 Mm, respectively.

(A color version of this figure is available in the online journal.)

the flow beneath 0.75 $R_\odot$ and enhance the S/N through the entire convection zone, and the capability of the shorter-time measurement allows us to study the temporal evolution of the deep meridional flow with lower S/N.

This new picture of the solar interior meridional circulation differs substantially from the previously widely believed picture of a single-cell circulation with the equatorward flow near the bottom of the convection zone. Through removing a systematic center-to-limb effect that was only recently identified, our analysis corrects and improves the previous solar interior meridional flow profile given by Giles (1999) using a similar analysis procedure. The new meridional circulation profile poses a challenge to the flux-transport dynamo models (Charbonneau 2010), but provides more physical constraints to these models creating a new opportunity to further understand how magnetic field is generated and how magnetic flux is transported inside the Sun. Past dynamo simulations have already demonstrated that a meridional circulation profile with multiple cells might not be able to reproduce the butterfly diagram and the phase relationship between the toroidal and poloidal fields as observed, unless the dynamo model was reconsidered (Jouve & Brun 2007). However, on the other hand, solar convection simulations have shown the possibility of multi-cell circulation with a shallow equatorward flow (e.g., Miesch et al. 2006; Käpylä et al. 2012; Guerrero et al. 2013), demonstrating that our analysis results are reasonable. Moreover, a recent dynamo simulation, with the double-cell meridional circulation profile incorporated, showed that the solar magnetic properties could be robustly reproduced after taking into consideration of turbulent pumping, turbulent diffusivity, and other factors (Pipin & Kosovichev 2013). All these studies, together with our observational results, suggest a rethinking of how the solar magnetic flux is generated and transported inside the Sun.

We thank the two anonymous referees whose comments help to improve the presentation and quality of this Letter. *SDO* is a NASA mission, and HMI project is supported by NASA contract NAS5-02139 to Stanford University.

REFERENCES

Baldner, C. S., & Schou, J. 2012, ApJL, 760, L1
Braun, D. C., & Birch, A. C. 2008, ApJL, 689, L161
Charbonneau, P. 2010, LRSP, 7, 3
Choudhuri, A. R., Schüssler, M., & Dikpati, M. 1995, A&A, 303, L29
Dikpati, M., & Charbonneau, P. A. 1999, ApJ, 518, 508
Dikpati, M., Gilman, P. A., de Toma, G., & Ulrich, R. K. 2010, GeoRL, 37, L14107
Duvall, T. L., Jr., Jefferies, S. M., Harvey, J. W., & Pomerantz, M. A. 1993, Natur, 362, 430
Giles, P. M. 1999, PhD thesis, Stanford Univ.
Giles, P. M., Duvall, T. L., Jr., Scherrer, P. H., & Bogart, R. S. 1997, Natur, 390, 52
Gizon, L., Birch, A. C., & Spruit, H. C. 2010, ARA&A, 48, 289
González Hernández, I., Kholikov, S., Hill, F., Howe, R., & Komm, R. 2008, SoPh, 252, 235
Gough, D., & Hindman, B. W. 2010, ApJ, 714, 960
Guerrero, G., Smolarkiewicz, P. K., Kosovichev, A., & Mansour, N. 2013, IAU Symp., 294, 417
Haber, D. A., Hindman, B. W., Toomre, J., et al. 2002, ApJ, 570, 855
Hartlep, T., Zhao, J., Kosovichev, A. G., & Mansour, N. N. 2013, ApJ, 762, 132
Hathaway, D. H. 2012, ApJ, 760, 84
Hathaway, D. H., & Rightmire, L. 2010, Sci, 327, 1350
Jiang, J., Chatterjee, P., & Choudhuri, A. R. 2007, MNRAS, 381, 1527
Jouve, L., & Brun, A. S. 2007, A&A, 474, 239
Käpylä, P. J., Mantere, M. J., & Brandenburg, A. 2012, ApJL, 755, L22
Komm, R. W., Howard, R. F., & Harvey, J. W. 1993, SoPh, 147, 207
Kosovichev, A. G. 1996, ApJL, 461, L55
Kosovichev, A. G., & Duvall, T. L., Jr. 1997, in Proc. of SCORe'96 Workshop, Solar Convection and Oscillations and Their Relationship, ed. F. P. Pijpers, J. Christensen-Dalsgaard, & C. S. Rosenthal (Dordrecht: Kluwer), 241
Miesch, M. S., Brun, A. S., & Toomre, J. 2006, ApJ, 641, 618
Mitra-Kraev, U., & Thompson, M. J. 2007, AN, 328, 1009
Paige, C. C., & Saunders, M. A. 1982, ACM Trans. Math. Software, 8, 43
Pesnell, W. D., Thompson, B. J., & Chamberlin, P. C. 2012, SoPh, 275, 3
Pipin, V. V., & Kosovichev, A. G. 2013, arXiv:1302.0943
Scherrer, P. H., Bogart, R. S., Bush, R. I., et al. 1995, SoPh, 162, 129
Scherrer, P. H., Schou, J., Bush, R. I., et al. 2012, SoPh, 275, 207
Schou, J., Scherrer, P. H., Bush, R. I., et al. 2012, SoPh, 275, 229
Švanda, M., Kosovichev, A. G., & Zhao, J. 2007, ApJL, 670, L69
Ulrich, R. K. 2010, ApJ, 725, 658
Wang, Y.-M., Nash, A. G., & Sheeley, N. R. 1989, Sci, 245, 712
Zhao, J., & Kosovichev, A. G. 2004, ApJ, 603, 776
Zhao, J., Nagashima, K., Bogart, R. S., Kosovichev, A. G., & Duvall, T. L., Jr. 2012, ApJL, 749, L5